Efficiency evaluation of VHC: a CFD comparison study at constant flow

Ricardo F. Oliveira, Senhorinha F. Teixeira, Helena C. Marques and José C. Teixeira

***Abstract*—**Background: The objective of this work is to numerically evaluate several commercial Valved Holding Chamber (VHC) geometries, in terms of airflow behavior and wall deposition. Also, the Fine Particle Dose (FPD) and Mass Mean Aerodynamic Diameter (MMAD) of the drug dose reaching the lungs were evaluated. Downwards the VHC Mouthpiece, the USP Throat geometry was added. Major detail was included in the VHC components representation.

Methods: Through the use of Computational Fluid Dynamics (CFD), the airflow velocity and turbulence fields were calculated for four geometries (i.e. A2A®, Aerochamber Plus® Flow-Vu®, NebuChamber© and Volumatic®). Using a constant flow of 30 L/min and several realistic spray inputs, the deposition was analyzed for three distinct particle size distributions.

Results: The Volumatic® presents the higher recirculation in comparison to the other small volume VHC devices. Each VHC Valve and Mouthpiece design leads to different flows entering the Throat, where the NebuChamber© exhibits the higher air velocities (i.e. 34 m/s). The higher is the MMAD of the distribution injected, the greater will be the deposition in the upper walls. Therefore, the lower MMAD distribution results in higher dose available for the patient. Volumatic® showed the higher Body deposition, as well as, the NebuChamber© USP Throat. Although the Aerochamber® Valve presents the higher deposition, it provides the greater amount of drug for the patient lungs.

On the other hand, the Volumatic® geometry while yielding the lower MMAD for the patient is far from providing the higher FPD.

Conclusions: Based on the results, the VHC components design lead to very distinct airflow patterns. The sudden changes in particle trajectory result in higher deposition at those locations. The Aerochamber® delivers the higher FDM to the patient lungs, while the Volumatic® delivers the smaller MMAD distribution to the lungs.

***Keywords*—** Asthma Treatment, Computational Fluid Dynamics (CFD), Deposition Efficiency, pressurized Metered Dose Inhaler (pMDI), Valved Holding Chamber (VHC).

I. Introduction

SINCE Ancient Egypt, when its use was first recorded[1], the goal of inhalation therapy is to improve breathing and lung function in order to relieve the symptoms of respiratory issues, such as asthma or other chronic obstructive pulmonary disease. Anti-inflammatory and bronchodilator drugs are used to reduce the inflammation of the pulmonary tissue, which causes a decrease of the bronchus diameter.[2] Developed in 1955[1], the pressurized Metered Dose Inhaler (pMDI) became one of the most common oral drug delivery devices used by the medical community in inhalation therapy. The pMDI is a compact, low cost and easy-to-use droplet spray dispenser for multiple-dose treatment.[3] A key component of the device is the actuator spray nozzle, which controls the atomization process and the resulting spray formation in terms of spray angle and droplet size distribution.[4], [5] pMDIs are characterized by high spray velocities which are responsible for the so called "cold-Freon" sensation in the patient's throat.[6] Plus, the use of this medical device requires coordination between the inspiratory action and pMDI priming. Not all patients have the capacity to use properly a pMDI. In fact, some patients may not be able of such hand-mouth coordination skill.[7], [8]

In order to solve the pMDI drawbacks, spacers were developed. Reports of the first spacer like devices date from 1956 and 1977.[6] They can be classified in three categories: a) simple tube, b) Valved Holding Chamber (VHC) and c) reverse flow.[6], [9] These add-on devices extend the distance between the pMDI and the patient's mouth and they contribute to the reduction of the high velocity impact of the spray on the throat and the need for inspiratory coordination. The one-way valve makes the normal respiratory cycle possible, by preventing the entrance of the exhalation flux into the VHC.[6], [10]

The VHC geometry influences the airflow pattern inside the device and, therefore, its treatment efficiency. By using Computational Fluid Dynamics (CFD) tools, it was possible to analyze and evaluate different aspects, as the airflow characteristics and drug deposition of the VHC devices. These CFD tools have the advantage to predict different geometric scenarios and evaluate its drug delivery efficiency with low

The first author would like to express his acknowledgments for the support given by the Portuguese Foundation for Science and Technology (FCT) through the PhD grant SFRH/BD/76458/2011. This work was financed by National Funds-Portuguese Foundation for Science and Technology, under Strategic Project PEst-C/EME/UI4077/2011 and PEst-OE/EME/UI0252/2011.

R. F. Oliveira is with the CT2M R&D center, Department of Mechanical Engineering, University of Minho, Guimarães, 4800-058 Portugal (corresponding author to provide e-mail: ricardo.falcao.oliveira@gmail.com).

S. F. Teixeira is with CGIT R&D center, Department of Production and Systems, University of Minho, Guimarães, 4800-058 Portugal (e-mail: st@dps.uminho.pt).

H. C. Marques is with the iMed.UL R&D center, Faculty of Pharmacy, University of Lisbon, Lisbon, 1649-003 Portugal (e-mail: hcmarques@ff.ul.pt).

J. C. Teixeira is with the CT2M R&D center, Department of Mechanical Engineering, University of Minho, Guimarães, 4800-058 Portugal (e-mail: jt@dem.uminho.pt).

investment by reducing the need for prototypes. Kleinstreuer and collaborators used CFD to evaluate the drug deposition in the airways with and without spacer.[11] Longest *et al.* also studied the effect of different breathing patterns, with both the pMDI and Dry Powder Inhaler (DPI) devices, on the aerosol delivery using numerical tools.[12] The application of CFD studies in the drug delivery scientific field is not new, although several topics still need to be explored as pointed out in the review of Ruzycki and collaborators.[13]

The CFD modeling of the pMDI spray is very challenging.[13] The physical events start with a multiphase fluid (composed by liquid propellant, excipients and particles of solid Active Pharmaceutical Ingredient - API[14]) stored at 3-5 atm[15], which suffers an initial expansion when dosed, resulting in a flash evaporation[5], [16] inside the plastic actuator. This is followed by a rapid expansion (which leads to high velocities and extreme turbulent multiphase flow assisted with cavitation[17]) running through the actuator nozzle and reaching the exit, becoming in full contact with the ambient air pressure and temperature. Studies show that the pMDI spray size distribution is influenced by the nozzle diameter, length and depth, by the concentration of the components in the mixture and the metered valve volume.[4], [15], [18] Cavitation will also change the droplets size in an unpredictable way, by the detachment of big agglomerates of API and propellant.[5] The ambient and the device temperature is of extreme importance for the spray characteristics, the mixture will rapidly decrease its pressure, absorbing all the energy in its vicinity to evaporate the propellant. The initial spray plume temperature at the nozzle exit is around -60 ºC.[19]–[21] Therefore, a higher environment temperature improves the propellant evaporation, resulting in smaller droplets and lower spray velocities. Even the delay between shaking and priming of the pMDI plays a major role in the spray plume characteristics, due to sedimentation by gravity.[22] Also, the spray plume shape is time-dependent, which can be observed by high-speed photography.[3], [9]

It is also known that a pMDI spray produces particles differently charged, due to the materials used in the device and the mixture components.[23] Combining this with the unpredictable wall charge of the VHC devices, makes it a very complex phenomenon to model numerically. The VHC wall charge can change: along the longitudinal position[23], for each type of material, with the detergent used to wash it[24], if it is handled with rubber gloves[25], with the friction during transportation[26], with the type of drying applied[24], also with the type of pMDI spray used[26], even with the number of puffs fired into it[25].

Due to the difficulties associated with the physical phenomena, all the CFD simulations are made by assuming some simplifications.

The main objective of this work is to evaluate four different geometries of commercial VHC devices in terms of velocity magnitude recirculation, and mass deposition in the VHC Body, Valve and USP Throat. Also, the Fine Particle Dose (FPD) and Mass Mean Aerodynamic Diameter (MMAD) of the drug sample that reaches the lungs are evaluated.

II. Materials and Methods

A. Geometry and Grid Generation

This paper reports a numerical fluid simulation in four different VHC geometries, based in commercial models (see Fig. 1): the A2A Spacer® from Clement Clarke International (210 mL), Aerochamber Plus® Flow-Vu® from Trudell Medical International (149 mL), NebuChamber© from AstraZeneca (250 mL) and Volumatic® from GlaxoSmithKline (750 mL).

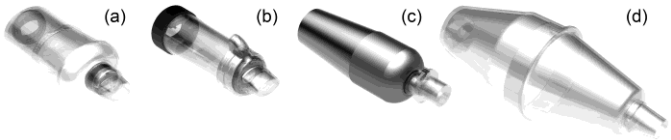

Fig. 1. Geometrical representation of the VHC geometries tested: (a) A2A®, (b) Aerochamber Plus® Flow-Vu®, (c) NebuChamber© and (d) Volumatic®.

After a computational representation of each VHC geometry, the USP Throat was added at the Mouthpiece of each device. Also a cross-sectional extension of the pMDI mouthpiece was added at the entry of each VHC geometry. Specifically in the Aerochamber® case, it was drawn the geometry of the flow warning whistle, close to the VHC pMDI adapter zone. This forced the need for a buffer extension at the VHC entrance for a proper calculation of the flow pressure drop.

The VHC geometries were draw considering all the details in the Body geometry. Also the Valves were considered to be in the open position at a flow of 30 L/min, for which the devices were connected to a vacuum pump with the calibrated flow. The approximate dimensions and shapes of the Valves were taken into account.

To reduce the computational effort, for each one of the numerical studies, only half of the geometry was simulated via a longitudinal symmetry plane.

The first step in a CFD simulation is the grid generation, for each geometry, taking advantage of the ANSYS Meshing software. The resulting 3D computational grids sizes, composed of tetrahedral elements, were 4.5, 4.8, 4.7, 1.6 (in millions of elements); for the A2A®, Aerochamber®, NebuChamber© and Volumatic® geometries, respectively. For 3D meshing of very complex geometries, the use of tetrahedral elements generally provides a more automatic solution, with the ability to add mesh controls for improving the accuracy in critical sections of the geometry. Thus, a refinement algorithm for proximity was used, in order to improve the solution accuracy. Plus, wall refinements were included to accurately solve the high velocity gradient.

For accuracy and mesh independency, a mesh size study was carried out using three different sizes of mesh elements, in the Volumatic® geometry. This study was done accordingly to the methodology proposed by Celik and his collaborators.[27]

ISBN: 978-1-61804-220-0

The same grid refinements were kept and the value of the velocity was evaluated in a cross-section located at half-length of the VHC Body, where the recirculation is bigger and the grid refinement is most important. Also, the velocity magnitude value for 5 points distributed along the VHC central axis of each geometry was monitored during the numerical iterations.

B. Boundary Conditions

The geometry inlet was defined as a boundary condition at atmospheric pressure with turbulence intensity assumed to be 5 %. A symmetry condition was imposed at the longitudinal symmetry plane. The outflow zone, located at the end of the USP Throat, imposed a constant draw of air flow (i.e. 30 L/min), which was defined by a uniform velocity profile with 2 % of turbulence intensity.

A no-slip condition was set for the geometry walls, which assumes that they have a fixed zero velocity value. These walls were separated in different groups, corresponding to different zones of the geometry for post-processing purposes.

C. Spray Simulation

For the particle calculations, it was considered that all the particles that collided with a wall would be trapped. This simplification does not represent the reality, but it would be the equivalent of having liquid droplets colliding to a dry wall. Although the reality of pMDI spray involves solid API particles trapped inside propellant liquid droplets, this approach seems to be acceptable even without considering evaporation.

For the definition of the pMDI spray, it was necessary to measure the parameters that were not readily available in the literature. Considering in a commercial pMDI HFA-134a device, the parameters considered are detailed in Table I.

TABLE I. PMDI SPRAY CHARACTERISTICS USED IN THE SIMULATIONS

Characteristic	Value
API	Salbutamol
Propellant	HFA-134a
Plume Max. Velocity (m/s)	90
Plume Angle (º)	22
Nozzle Diameter (mm)	0.25
API Mass (μg)	100
Plume Duration (s)	0.1
Salbutamol Density (kg/m^3)	1230
Size Distribution	Log-Normal

In Table II, the three different types of size distribution characteristics simulated for each geometry are reported. The distributions are characterized by their MMAD and Geometric Standard Deviation (GSD). A graphical representation of the sprays can be found in Fig. 2.

TABLE II. SPRAY DISTRIBUTION SIZE CHARACTERISTICS USED IN THE SIMULATIONS

Distribution Number	1	2	3
MMAD (μm)	2.28	5.47	14.0
GSD	1.35	1.50	1.80

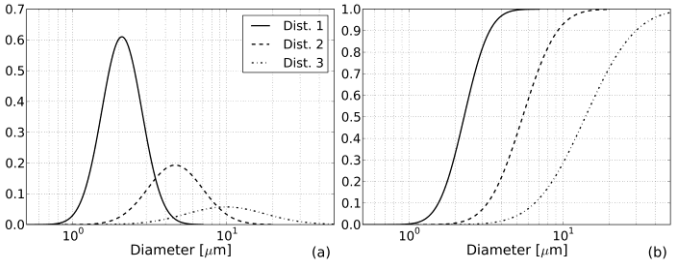

Fig. 2. Representation of the three particle size distributions used in the simulations. Log-Normal forms: (a) distributed and (b) cumulative.

These distributions were selected with the purpose of testing the effect of MMAD increase in the deposition, but keeping the same spray shape and the total mass amount of API (i.e. 100 μg). The simulations did not include the evaporation of the propellant (i.e. the particles are considered to be solid) and the collision with a wall assumes certain retention. Therefore, it was important to consider three distinct scenarios: Dist. 1 – a characteristic distribution of the solid API particles that can be measured in a Cascade Impactor (CI); Dist. 3 – represents the expected size distribution of a pMDI spray before the evaporation of the propellant that can be measured by laser diffraction; and Dist. 2 – represents a distribution that should be an average between the two other cases.

Through the Python language, a script was programmed. It contained mathematical operations for the creation of an injection file using the characteristics reported in Tables I and II. In addition, the spray was considered to have a conical shape, and that the particles exiting the circular section of the nozzle were randomly distributed within it. This injection file is the spray input into the CFD solver. More details regarding the pMDI spray simulation can be found elsewhere.[3], [28]

D. Solver Configuration

The numerical simulations were performed using FLUENT 14.0 from ANSYS® as the solver. FLUENT software uses a control volume technique to solve the conservation equations for mass, momentum and turbulence measurements.[29], [30] Concerning the turbulence calculations, a two-equation model was used, known as the *k-ε* Standard. Also the Standard algorithm was used for the calculation of the boundary layer.[30] The solution of the partial differential equations for mass and momentum was defined in a sequential process, using the SIMPLE (or Semi-Implicit Method for Pressure-Linked Equations) algorithm. The standard discretization scheme was used to solve the pressure field whereas the momentum, the turbulent kinetic energy and turbulent dissipation rate equations were discretized by applying the second order upwind scheme. Convergence was reached in the simulation by using a criterion value of 1.0E-6 for the

ISBN: 978-1-61804-220-0

continuity (pressure), velocity, and for k and ε turbulence parameters. The simulation was obtained in steady state and the fluid was assumed incompressible and Newtonian. There is no energy exchange and the gravitational acceleration was applied with a magnitude value of 9.81 m/s^2.

For the particle tracking within the velocity domain, an Euler-Lagrangian approach was used. The tracking was executed after the numerical convergence of the continuous phase has been reached. A drag coefficient law based in the work of Morsi and Alexander[30] was used with a correction for the Cunningham Slip effect for particles under 1 μm of diameter.[20], [31] A model for statistically simulate the turbulence effect on particle trajectory, known as stochastic tracking, was used. Five stochastic paths were considered for each particle tracking with different random turbulence eddy number. No electrostatic or evaporation effects were taken into account during the particle tracking calculations.

E. Post Processing

The grid computed numerical fields were evaluated in terms of velocity magnitude and pathlines, by using the CFD-Post program suite from ANSYS.

For evaluating the four VHC devices, the mass deposition fraction in the Body, Valve and USP Throat was calculated. Also the fraction that exited the geometry to the lungs, as well as, its MMAD and FPD, were calculated. These metrics were quantified through a Python language script by several mathematical operations, having as input the deposition wall files from the CFD studies.

III. Results

A. Velocity Contours

Fig. 3 presents the CFD results for the velocity magnitude contours, obtained at the symmetry plane of each one of the four geometries. The results are plotted in a logarithmic greyscale and expressed in m/s. The airflow is drawn through the USP Throat exit at 30 L/min.

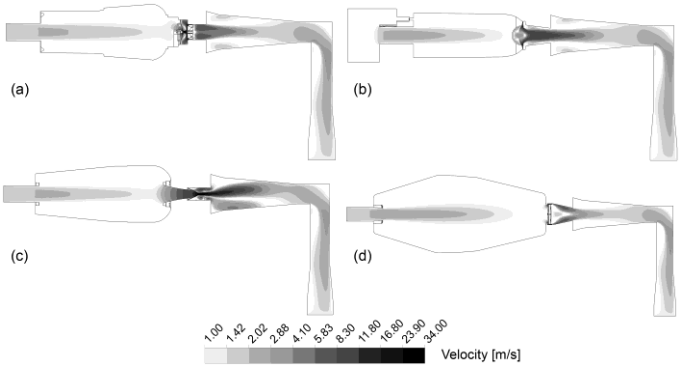

Fig. 3. Velocity magnitude contours for the symmetry plane of each geometry: (a) A2A®, (b) Aerochamber®, (c) NebuChamber© and (d) Volumatic®. Results are represented in m/s in a logarithmic greyscale, for a flow of 30 L/min.

B. Airflow Pathlines

Taking the VHC Body section of the geometry and plotting the velocity magnitude contours along with the airflow pathlines, the results shown in Fig. 4 were obtained. The pathlines provide a better pattern perception into the level of recirculation created by each geometry, as the airflow is kept at 30 L/min.

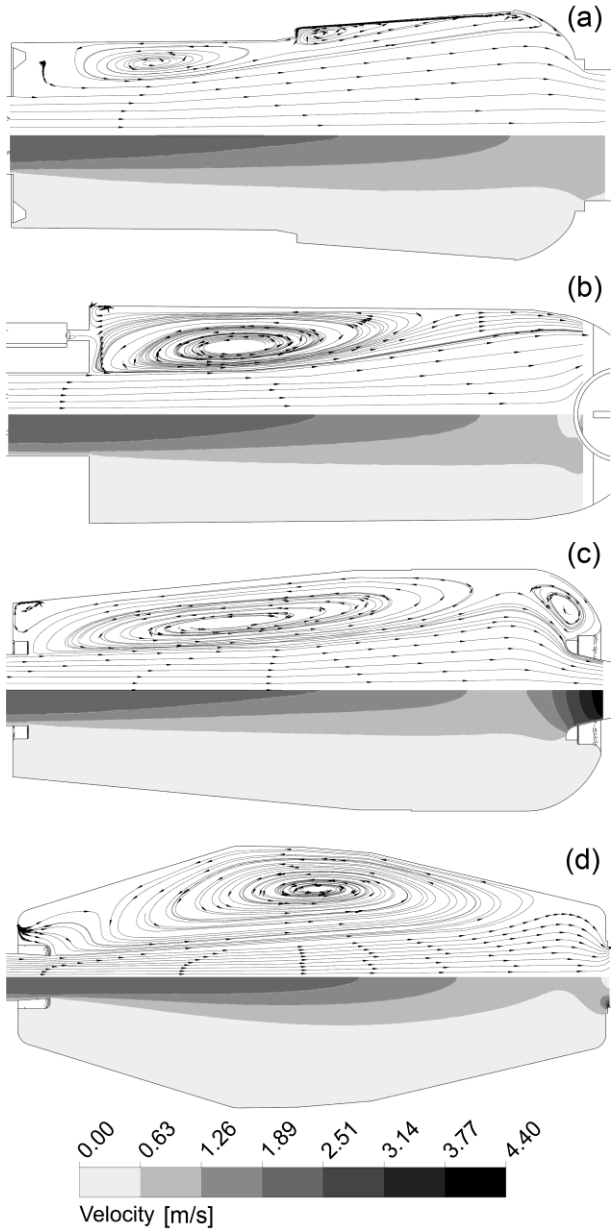

Fig. 4. Representation of the airflow pathlines inside the VHC body, along with the velocity magnitude contour for the following geometries: (a) A2A®, (b) Aerochamber®, (c) NebuChamber© and (d) Volumatic®. Velocity results shown in m/s, for a flow of 30 L/min.

In Fig. 5, some randomly seeded pathlines in a cross-section plane upstream the Valve of each geometry are represented. It is possible to observe the direction of the flow as well as the different designs of each Valve and Mouthpiece simulated.

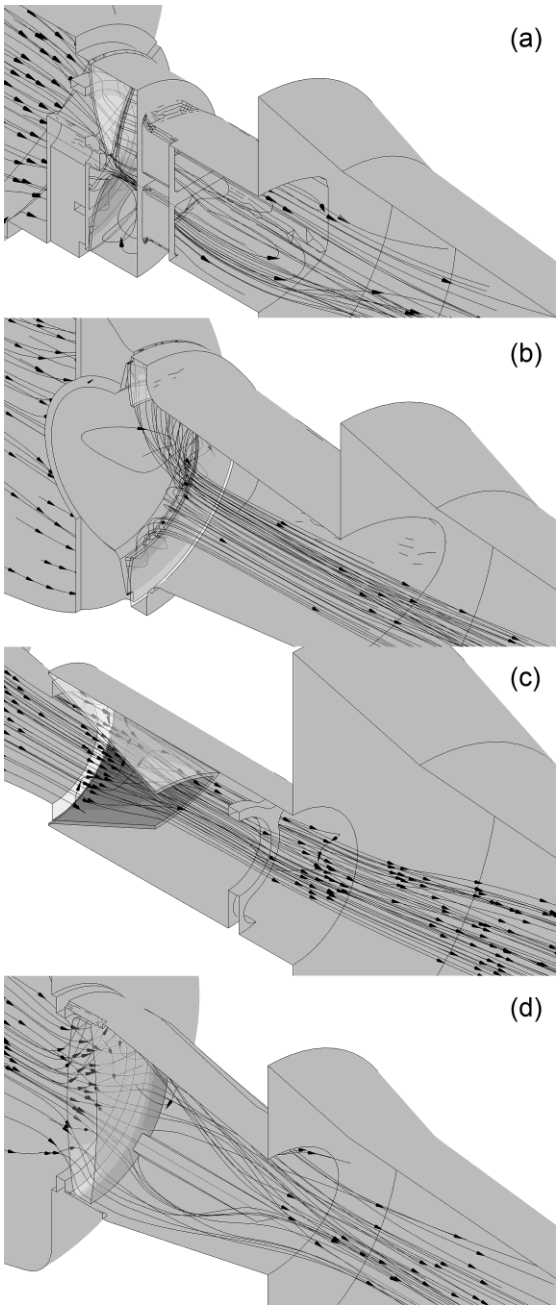

Fig. 5. Detail of the VHC valves flow pathlines for the devices: (a) A2A®, (b) Aerochamber®, (c) NebuChamber© and (d) Volumatic®. The valve surfaces drawn with a 60% of transparency, and the arrows indicate the direction of the flow.

C. Particle Deposition

Fig. 6 reports the mass fraction deposition results in relation to the total mass emitted (i.e. 100 μg), for each zone and geometry. Results are expressed in percentage for a constant flow of 30 L/min. The zone "To Lungs" represents the amount of drug that exits the USP Throat and, therefore, leaves the domain. This amount of drug will be the same entering the CI device. This is represented in this easy way for experimental comparison and better understanding of the drug delivery effectiveness to the patient lungs.

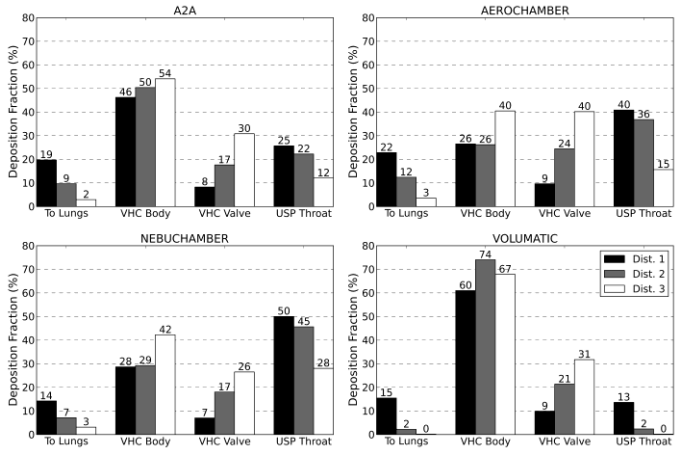

Fig. 6. Representation of the deposition fraction for the three distributions at the four zones, in four VHC geometries. Results shown in percentage at 30 L/min.

In Fig. 7 (a), the MMAD and GSD (in vertical alignment inside the bars) of the amount of drug dose that reaches the lungs are shown. The effective fraction of the emitted dose (i.e. FPD) that reaches the lungs is also represented in Fig. 7 (b). Both are characterized for a constant flow of 30 L/min, for each distribution and VHC geometry.

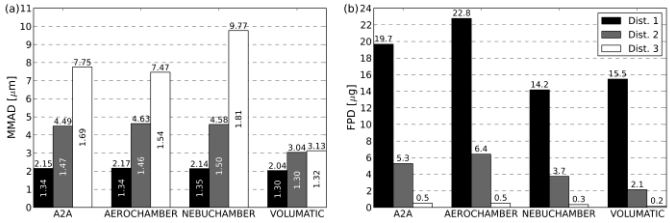

Fig. 7. (a) Values of MMAD and GSD and (b) FPD drug amount, both obtained for each VHC geometry and for three different size distributions. The values were taken from the dose reaching the lungs at a flow of 30 L/min.

IV. Discussion

A. Velocity

It can be observed, in Fig. 3, that the (c) NebuChamber© geometry shows higher velocities downwards the Valve, at a value of around 34 m/s. This can be explained by the small cross-section area of the NebuChamber© Valve (see Fig. 5 (c)), which results in a higher drug deposition in the USP Throat walls (see Fig. 6).

The (b) Aerochamber® and (d) Volumatic® geometries show lower velocity values, around 13 m/s. Their Valve and Mouthpiece design is simpler and include less obstacles, having a higher cross-section area (see Fig. 5 (b) and (d)) that results in lower velocities.

For the USP Throat velocity contours a similarity is found for Fig. 3 (a), (b) and (d) geometries, due to their air jet being aligned with the USP Throat centerline. On the other hand, the (c) NebuChamber© shows a distinct behavior, where the jet appears to be aiming towards the wall.

ISBN: 978-1-61804-220-0

B. Recirculation

Observing Fig. 4, it can be concluded that different VHC Body geometries lead to different airflows and therefore distinct recirculation patterns. The (d) Volumatic® has the widest recirculation area, as expected, due to its high volume in comparison to the other geometries considered in this study. Such large recirculation zone can be the reason of the high deposition in the VHC Body when compared with the other devices, see Fig. 6.

The (a) A2A® geometry presents multiple small area recirculation zones. For the (c) NebuChamber© geometry, it is visible a major recirculation zone plus two other smaller ones, formed in the vicinity of wall recesses.

In the (b) Aerochamber® geometry, it is visible a single recirculation area located downstream the VHC entrance, caused for sudden expansion. Even the whistle entrance modeled did not provide a meaningful influence in this recirculation zone.

C. Deposition

By observing the results in Fig. 6, it can be concluded that the deposition is greater in the Volumatic® Body than in the other VHC's bodies. On the other hand, the Aerochamber® Valve yields the largest Valve deposition. The NebuChamber© geometry results in a greater USP Throat deposition than the other VHCs. Also the Aerochamber® VHC leads to the greatest amount of delivered drug that reaches the lungs.

Analyzing the different distributions, it can be noticed that Dist. 1 presents a higher amount of drug reaching the lungs in comparison to the other distributions. This is an expected result since the Dist. 1 has the lower MMAD, and as it is well known, particles with lower diameter are most likely to follow the flow stream and not collide with solid obstacles. On the other hand, Dist. 3 presents the highest deposition in the VHC walls (i.e. Body and Valve) and therefore the lowest amount of drug delivered to the lungs. As explained before, because Dist. 3 exhibits the highest emitted MMAD, this results in higher deposition.

Due to the fact that no evaporation has been considered and that a 100% probability of retention is assumed in case of a particle-wall collision, the results may be an over prediction of the reality. On the other hand, the fact that no electrostatic effects have been considered, the deposition for low diameter particles may be under predicted.

D. MMAD and GSD

From Fig. 7 (a) it can be concluded that injected spray distributions with higher MMAD results in higher MMAD delivered to the lungs, although there is a general reduction of its original MMAD value, as well as, the GSD value. This is expected due to the fact that the coarse fraction of the distribution has higher probability to get trapped in the domain walls, resulting in a lowering of the MMAD and GSD values.

Comparatively between all the VHCs, the Volumatic® shows the highest reduction of MMAD from the initial injected distribution. This is a great reduction in comparison to the other geometries, and surely is related to the fact that Volumatic® is a higher volume VHC than the other three, which are of similar volume. NebuChamber© presents the lowest reduction in the MMAD value from the initial distribution, making it the less attractive for patient treatment. Nonetheless, it must be kept in mind that this VHC device is the only one made of metal, the results are less likely to be affected by the electrostatic forces on the deposition. Aerochamber® and A2A® present similar distributions delivered to the lungs.

E. Fine Particle Dose

Fig. 7 (b) provides an insight from the clinical point of view into the amount of dose that reaches the lung, by evaluating the fraction with diameter lower than 4.7 μm. The results show that the lower MMAD emitted distribution (i.e. Dist. 1) results in higher FPD reaching the lungs, independently of the geometry.

For all the distributions, the Aerochamber® presents the highest FPD values, which for the conditions considered in the simulation appears to provide the best option for treatment, followed by the A2A®. Conversely, the NebuChamber© shows the lowest value of FPD.

The combination of the several results shows that despite the fact that the Volumatic® geometry presents the lower MMAD for the patient, it does not guarantee the higher FPD. As well as, the fact of the NebuChamber© has the lower Body and Valve deposition is far from having the higher FPD and lower MMAD, but has the higher USP Throat deposition.

REFERENCES

[1] M. Sanders, "Inhalation therapy: an historical review," *Prim. care Respir. J.*, vol. 16, no. 2, pp. 71–81, Apr. 2007.

[2] Global Initiative for Asthma, "Global strategy for asthma management and prevention," GINA, 2012.

[3] R. F. Oliveira, S. F. C. F. Teixeira, J. C. Teixeira, L. F. Silva, and H. Antunes, "pMDI Sprays: Theory , Experiment and Numerical Simulation," in *Advances in Modeling of Fluid Dynamics*, C. Liu, Ed. Rijeka, Croatia: Intech, 2012, p. 300.

[4] H. Smyth, A. J. Hickey, G. Brace, T. Barbour, J. Gallion, and J. Grove, "Spray pattern analysis for metered dose inhalers I: Orifice size, particle size, and droplet motion correlations," *Drug Dev. Ind. Pharm.*, vol. 32, no. 9, pp. 1033–1041, Oct. 2006.

[5] C. A. Dunbar, "Atomization mechanisms of the pressurized metered dose inhaler," *Part. Sci. Technol.*, vol. 15, no. 3–4, pp. 253–271, Jul. 1997.

[6] S. P. Newman, "Spacer devices for metered dose inhalers," *Clin. Pharmacokinet.*, vol. 43, no. 6, pp. 349–360, Jan. 2004.

[7] M. B. Dolovich and R. Dhand, "Aerosol drug delivery: developments in device design and clinical use," *Lancet*, vol. 377, no. 9770, pp. 1032–1045, Mar. 2011.

[8] J. B. Fink, "Metered-dose inhalers, dry powder inhalers, and transitions," *Respir. Care*, vol. 45, no. 6, pp. 623–635, Jun. 2000.

[9] C. Terzano, "Pressurized metered dose inhalers and add-on devices.," *Pulm. Pharmacol. Ther.*, vol. 14, no. 5, pp. 351–66, Jan. 2001.

[10] M. B. Dolovich and J. B. Fink, "Aerosols and devices," *Respir. Care Clin. N. Am.*, vol. 7, no. 2, pp. 131–173, Jun. 2001.

[11] C. Kleinstreuer, H. Shi, and Z. Zhang, "Computational analyses of a pressurized metered dose inhaler and a new drug-aerosol targeting methodology," *J. aerosol Med.*, vol. 20, no. 3, pp. 294–309, Jan. 2007.

[12] P. W. Longest, G. Tian, R. L. Walenga, and M. Hindle, "Comparing MDI and DPI aerosol deposition using in vitro experiments and a new

stochastic individual path (SIP) model of the conducting airways," *Pharm. Res.*, vol. 29, no. 6, pp. 1670–88, Jun. 2012.
[13] C. A. Ruzycki, E. Javaheri, and W. H. Finlay, "The use of computational fluid dynamics in inhaler design," *Expert Opin. Drug Deliv.*, vol. 10, no. 3, pp. 307–23, Mar. 2013.
[14] S. W. Stein, P. Sheth, and P. B. Myrdal, "A model for predicting size distributions delivered from pMDIs with suspended drug," *Int. J. Pharm.*, vol. 422, no. 1–2, pp. 101–15, Jan. 2012.
[15] S. P. Newman, "Principles of metered-dose inhaler design.," *Respir. Care*, vol. 50, no. 9, pp. 1177–1190, Sep. 2005.
[16] A. Q. Shaik, "Numerical modeling of two-phase flashing propellant flow inside the twin-orifice system of pressurized metered dose inhalers," Loughborough University, 2010.
[17] C. A. Dunbar, A. P. Watkins, and J. F. Miller, "An experimental investigation of the spray issued from a pMDI using laser diagnostic techniques," *J. Aerosol Med.*, vol. 10, no. 4, pp. 351–68, Jan. 1997.
[18] S. W. Stein, "Estimating the number of droplets and drug particles emitted from MDIs.," *AAPS PharmSciTech*, vol. 9, no. 1, pp. 112–5, Jan. 2008.
[19] S. W. Stein and P. B. Myrdal, "The Relative Influence of Atomization and Evaporation on Metered Dose Inhaler Drug Delivery Efficiency," *Aerosol Sci. Technol.*, vol. 40, no. 5, pp. 335–347, Jun. 2006.
[20] W. H. Finlay, *The mechanics of inhaled pharmaceutical aerosols: an introduction*. Academic Press, 2001, p. 306.
[21] B. J. Gabrio, S. W. Stein, and D. J. Velasquez, "A new method to evaluate plume characteristics of hydrofluoroalkane and chlorofluorocarbon metered dose inhalers.," *Int. J. Pharm.*, vol. 186, no. 1, pp. 3–12, Sep. 1999.
[22] E. Berg, "In vitro properties of pressurized metered dose inhalers with and without spacer devices.," *J. Aerosol Med.*, vol. 8, no. Supplement 3, pp. S3–S11, Sep. 1995.
[23] P. C. L. Kwok, R. Collins, and H.-K. Chan, "Effect of spacers on the electrostatic charge properties of metered dose inhaler aerosols," *J. Aerosol Sci.*, vol. 37, no. 12, pp. 1671–1682, Dec. 2006.
[24] J. H. Wildhaber, S. G. Devadason, M. J. Hayden, R. James, A. P. Dufty, R. A. Fox, Q. A. Summers, and P. N. LeSouëf, "Electrostatic charge on a plastic spacer device influences the delivery of salbutamol," *Eur. Respir. J.*, vol. 9, no. 9, pp. 1943–1946, Sep. 1996.
[25] N. J. Dewsbury, C. J. Kenyon, and S. P. Newman, "The effect of handling techniques on electrostatic charge on spacer devices: A correlation with in vitro particle size analysis," *Int. J. Pharm.*, vol. 137, no. 2, pp. 261–264, Jun. 1996.
[26] P. C. L. Kwok, "Electrostatics of Aerosols for Inhalation," University of Sydney, 2007.
[27] I. B. Celik, U. Ghia, P. J. Roache, C. J. Freitas, H. Coleman, and P. E. Raad, "Procedure for Estimation and Reporting of Uncertainty Due to Discretization in CFD Applications," *J. Fluids Eng.*, vol. 130, no. 7, pp. 1–4, 2008.
[28] R. F. Oliveira, A. C. M. Ferreira, S. F. C. F. Teixeira, J. C. Teixeira, and H. M. C. Marques, "pMDI Spray Plume Analysis: A CFD Study," in *Lecture Notes in Engineering and Computer Science: Proceedings of The World Congress on Engineering 2013, WCE 2013*, 2013, vol. 3, pp. 1883–1888.
[29] H. K. Versteeg and W. Malalasekera, *An introduction to computational fluid dynamics: the finite volume method*. Harlow, England: Longman, 1995, p. 257.
[30] ANSYS, *ANSYS FLUENT Theory Guide*. Canonsburg, PA, USA: ANSYS Inc, 2011, p. 794.
[31] P. W. Longest and J. Xi, "Effectiveness of Direct Lagrangian Tracking Models for Simulating Nanoparticle Deposition in the Upper Airways," *Aerosol Sci. Technol.*, vol. 41, no. 4, pp. 380–397, Mar. 2007.